Noise in nearly-single-mode semiconductor lasers

George Gray and Rajarshi Roy
School of Physics, Georgia Institute of Technology, Atlanta, Georgia 30332
(Received 24 February 1989)

We report the results of a numerical study of nearly-single-mode semiconductor lasers. The stochastic nonlinear dynamical equations of the field and population inversion are integrated and the intensity fluctuations and line shapes of the laser are investigated. The second mode affects the coherence of the light output appreciably, particularly near the laser threshold regime. The accuracy of the linearized theory for a single-mode laser is tested from far below to far above threshold. It is found to be very accurate both far below and far above threshold, but significant discrepancies are seen in the threshold region. We automatically include the coupling of the intensity and phase fluctuations in the line-shape calculations, resulting in the experimentally observed asymmetry of the relaxation oscillation sidebands. The numerical technique developed here is easily applicable to multimode lasers and is shown to be a convenient and powerful probe of the coherence properties of semiconductor lasers.

I. INTRODUCTION

The necessity to develop monochromatic semiconductor lasers for coherent communications has focused great interest on the study of semiconductor-laser linewidth. Numerous papers have investigated experimentally and theoretically the noise characteristics of these devices. Until a few years ago, almost all the studies were restricted to linearized treatments of the semiconductor-laser rate equations. The linearized treatments were motivated by a desire to obtain an analytic result for the laser linewidth or intensity noise spectrum that would provide an accurate description above threshold. The experimental and theoretical work on single-mode laser linewidth has been reviewed recently by Henry.[1] Most of the theoretical treatments used linearized, semiclassical, Langevin equations to describe the laser behavior. These equations do an admirable job of explaining most of the characteristics of semiconductor lasers. This approach to semicon- ductor-laser noise phenomena is explained throughly by Agrawal in Ref. 2.

For many purposes, such a linearized treatment is perfectly adequate, and works particularly well far above laser threshold. It is important, however, to assess the limits of validity of this approach. Such a check requires that we develop a technique to calculate numerically the solutions of coupled, nonlinear Langevin equations. Such a numerical method would allow us to retain the full complexity of the semiconductor-laser equations and not assume that the fluctuations represent only small deviations from average steady-state values.

While a linearized treatment of single-mode operation is fairly simple analytically, multimode operation may present insurmountable difficulties. Further, there is always the danger that we may overlook qualitatively different aspects of laser behavior if we linearize a set of coupled nonlinear equations. This is particularly true when examining the effect of external reflections back into the laser cavity. In this case the equations are intrinsically nonlinear, and a linearized version of the theory will not capture the important aspects of observed behavior. Analytic solutions to such problems can rarely be obtained if the full nonlinearity is to be retained in the description.[3]

The solution of the semiconductor-laser equations by numerical techniques has been studied by several groups. Marcuse has undertaken a major effort to derive systematically the Langevin equations from the underlying quantum theory,[4–6] and has investigated the photon number fluctuations of a variety of semiconductor lasers by the technique of Monte Carlo simulations. Miller has developed a somewhat different approach to the simulations and has concentrated on design strategies for semiconductor lasers.[7–9] Jensen *et al.* have studied mode partition noise by a method similar to that of Marcuse.[10]

A motivation for the work presented here is to study aspects of the laser intensity fluctuations that illustrate the regime where nonlinear effects become important, i.e., near the threshold region. We compare the numerical results wherever possible with results of the linearized theory to delineate its limits of accuracy. The second major motive is to develop a technique for the study of the laser line shape by Monte Carlo simulations. This, to our knowledge, has not been attempted before.

It is an idealization to assume that a laser is single mode. In reality there is always present a small amount of light emitted by one or more side modes, in addition to the dominant mode. The coupling between such modes is through the gain of the laser, which includes self- and cross-saturation terms. The effect of the side mode on the intensity fluctuations is appreciable even when the mode-suppression ratio (ratio of the side mode to main mode power) is as small as 0.01. The fluctuation characteristics near threshold are rather different from the single-mode model and are not within the domain of analytic theory. The calculation of the laser line shape is

particularly intractable when more than one mode is involved. We show that it is very feasible to obtain line shapes for the nearly-single-mode laser (or multimode laser) from computer simulations.

We sketch the derivation of the basic equations utilized in the simulations in Sec. II. Though the photon number and phase equations have traditionally been employed in theory and simulations, we use the field equations here, since they lead much more naturally to the line shape.

The numerical procedure for the integration of the equations is described in Sec. III, as well as the calculation of the correlation functions and spectra.

In Sec. IV we consider the laser intensity noise. Relative intensity noise spectra, auto- and cross correlations, and the variance of the intensity fluctuations are obtained and compared to linearized theory.

Section V is concerned with line shapes and linewidths of the laser modes. We discuss line shifts as well, and the question of the power-independent linewidth. The appearance of satellite peaks due to relaxation oscillations and their asymmetry are studied. The line shape of the side mode is investigated.

We conclude with a brief discussion of the results and topics for further study in Sec. VI.

II. EQUATIONS FOR A TWO-MODE SEMICONDUCTOR LASER

The standard procedure[2] for the derivation of the semiclassical laser equations begins with the Maxwell equations. The complex electric field is analyzed in terms of cavity modes, either traveling or standing waves, as is the polarization of the active medium. An equation is obtained for the slowly varying field amplitude after substitution into the wave equation. In this process, higher-order derivatives and products of derivatives of the field and polarization are neglected. The polarization of the medium is expressed as a product of the electric field and the complex susceptibility of the semiconductor, which is dependent on the mode amplitude. The real part of the susceptibility determines the refractive index while the imaginary component is responsible for the gain. The electric field equations for the two-mode laser obtained in this fashion are

$$\frac{dE_1}{dt} = iF_{\mathrm{mm}}E_1 + \tfrac{1}{2}(G_1-\gamma_1)(1-i\beta_c)E_1 \ , \tag{1}$$

$$\frac{dE_2}{dt} = iF_{mm}E_2 + \tfrac{1}{2}(G_2-\gamma_2)(1-i\beta_c)E_2 \ . \tag{2}$$

E_1 and E_2 are the complex, slowly-varying components of the electric fields of the main and side modes. These fields are scaled such that they are dimensionless and

$$P_1 = |E_1|^2 \ , \tag{3a}$$

$$P_2 = |E_2|^2 \ , \tag{3b}$$

are the photon numbers of the main and side modes. F_{mm} is the angular frequency mismatch between the cavity modes and the actual laser oscillation frequencies. These are assumed equal for the main and side modes. γ_1 and γ_2 are the losses of the two modes and consist of the internal loss as well as the output coupling of the modes. β_c is the linewidth enhancement factor usually defined as

$$\beta_c = \frac{d\chi_r/dN}{d\chi_i/dN} \ , \tag{4}$$

where χ_r and χ_i are the real and imaginary components of the susceptibility of the semiconductor medium. N is the electron number in the laser active region. An overview of this linewidth enhancement factor, the importance of which was first realized by Henry, and Yariv and his co-workers, has recently been given by Osinski and Buus.[11] G_1 and G_2 are the gains associated with the main and side modes, and are given by the following expressions:[12]

$$G_1 = A(N-N_0) - \beta_{11}P_1 - \theta_{12}P_2 \ , \tag{5}$$

$$G_2 = A(N-N_0) - \beta_{22}P_2 - \theta_{21}P_1 - \delta G \ . \tag{6}$$

N_0 is the electron number necessary to achieve transparency of the active medium. β_{11} and β_{22} are mode self-saturation coefficients. θ_{12} and θ_{21} are the cross-saturation coefficients. Spectral hole burning is a physical mechanism responsible for the gain saturation. The cross-saturation terms depend on the frequency separation of the modes. δG is the gain rolloff, i.e., the decrease in gain as we depart from the gain peak of the active medium. A is the laser gain coefficient, given by

$$A = (\Gamma c a/\mu V) \ , \tag{7}$$

where a is determined phenomenologically from the slope of the linear gain versus injected carrier density plot. Γ is the mode confinement factor,[2] μ is the group refractive index, V is the volume of the active region, and c is the velocity of light in vacuum.

In addition to the time variation of the electric fields, we need the rate equation for the population inversion. The inversion is dependent on the injection current I as given below

$$\dot{N} = (I/q) - \gamma_e N - G_1P_1 - G_2P_2 \ , \tag{8}$$

where q is the electron charge, and γ_e is the carrier recombination rate. This rate is dependent on several mechanisms

$$\gamma_e = A_{\mathrm{nr}} + Bn + C_{\mathrm{Aug}}n^2 \ , \tag{9}$$

where A_{nr} is the nonradiative contribution arising from impurities and traps, B is the radiative decay coefficient, and C_{Aug} is the decay coefficient due to Auger processes. n is the electron density (N/V).

We will use the three coupled equations (1), (2), and (8) to determine the time evolution of the laser fields. These equations are, however, deterministic in nature and provide no information about the intensity or phase fluctuations. The semiclassical equations have to be augmented with noise sources in order to obtain statistical fluctuations of the laser field and population inversion. The derivation of the noise sources and their statistical properties is quantum mechanical. As Lax[13] and Marcuse[4]

have shown, it is necessary to quantize the fields to obtain the correlation functions of the noise sources. The noise sources added to the right-hand side of Eqs. (1), (2), and (8) are F_1, F_2, and F_N. F_1 and F_2 are complex noise sources while F_N is real. All these noise sources are Gaussian and have zero mean. The correlation functions for the field sources are

$$\langle F_i(t)F_j(t')\rangle = 2D_{ij}\delta(t-t')\delta_{ij} , \tag{10}$$

where i and j refer to subscripts 1 and 2. The noise strengths D_{ij} (which depend only on the steady-state average values of the variables) are given by

$$D_{11} = (R_{\rm sp}/2) = D_{22} . \tag{11}$$

$R_{\rm sp}$ is the rate of spontaneous emission coupled into each mode. This is assumed to be equal for the two modes, since the spontaneous-emission spectrum is extremely broad compared to the mode spacing. Quantitatively,

$$R_{\rm sp} = \beta_{\rm sp} B N^2 / V , \tag{12}$$

where $\beta_{\rm sp}$ is a coefficient determined by the lateral guiding mechanism of the laser.[2] The correlation function for F_N is

$$\langle F_N(t)F_N(t')\rangle = 2[R_{\rm sp}(\langle P_1\rangle + \langle P_2\rangle) + \gamma_e N]\delta(t-t') . \tag{13}$$

In addition to these autocorrelation functions, it is found that the noise sources F_i and F_N are correlated as well. These cross-correlation functions are

$$\langle F_{iR}(t)F_N(t')\rangle = \frac{R_{\rm sp}}{2}\sqrt{\langle P_i\rangle}\,\delta(t-t') , \tag{14a}$$

$$\langle F_{iI}(t)F_N(t')\rangle = \frac{R_{\rm sp}}{2}\sqrt{\langle P_i\rangle}\,\delta(t-t') . \tag{14b}$$

F_{iR} and F_{iI} are the real and imaginary components of the noise sources for the electric fields of the two modes and i refers to the mode index. In these and later equations, the strengths of the noise sources are defined by the steady-state ensemble averages for the variables, indicated by the angular brackets.

With the inclusion of the noise sources, the Langevin equations account for the fluctuations of the fields and population inversion. There are several physical (quantum-mechanical) origins for the noise sources that we have just described. The terms F_i include the effect of the commutation relation for the fermion operators of the electrons, since an adiabatic elimination of the dipole moment has been performed. The internal loss and output coupling contribute as well to the F_i. Pump fluctuations and spontaneous emission are responsible for the noise source F_N, which also has a contribution from the adiabatic elimination of the dipole moment. This adiabatic elimination of the dipole moment is thus the cause of the cross correlation between the F_i and F_N.

The conventional equations for the intensity and phase of the laser light are obtained from Eqs. (1) and (2) by using the definitions

$$E_1 = \sqrt{P_1}\,e^{-i\phi} , \tag{15a}$$

$$E_2 = \sqrt{P_2}\,e^{-i\psi} , \tag{15b}$$

where ϕ and ψ are the phases of the electric fields of the two modes. The intensity equations thus obtained are

$$\dot{P}_1 = (G_1-\gamma_1)P_1 + R_{\rm sp} + F_{P_1} \tag{16}$$

and

$$\dot{P}_2 = (G_2-\gamma_2)P_2 + R_{\rm sp} + F_{P_2} \tag{17}$$

where

$$\langle F_R(t)F_l(t')\rangle = 2D_{Rl}\delta(t-t'), \quad k,l = P_1,P_2,N . \tag{18}$$

The nonzero diffusion coefficients are

$$D_{P_1P_1} = R_{\rm sp}\langle P_1\rangle , \tag{19a}$$

$$D_{P_2P_2} = R_{\rm sp}\langle P_2\rangle , \tag{19b}$$

$$D_{P_1N} = -R_{\rm sp}\langle P_1\rangle , \tag{19c}$$

$$D_{P_2N} = -R_{\rm sp}\langle P_2\rangle . \tag{19d}$$

The accompanying phase equations are

$$\dot{\phi} = F_{mm} + \tfrac{1}{2}\beta_c(G_1-\gamma_1) + F_\phi , \tag{20}$$

and

$$\dot{\psi} = F_{mm} + \tfrac{1}{2}\beta_c(G_2-\gamma_1) + F_\psi , \tag{21}$$

where the noise sources F_ϕ and F_ψ are correlated as follows:

$$\langle F_\phi(t)F_\phi(t')\rangle = (R_{\rm sp}/2\langle P_1\rangle)\delta(t-t') , \tag{22}$$

$$\langle F_\psi(t)F_\psi(t')\rangle = (R_{\rm sp}/2\langle P_2\rangle)\delta(t-t') . \tag{23}$$

In conjunction with the population inversion equation, either the field or the intensity and phase equations may be used to determine the fluctuation characteristics of the laser. However, for the calculation of specific quantities, one or the other set is more appropriate. We will indicate in the remaining sections when this is so.

Typical values for $In_xGa_{1-x}As$:P lasers whose behavior we wish to model are given in Table I. More extensive tables for laser parameters are contained in Fig. 2.

III. NUMERICAL SIMULATION PROCEDURE

In order to obtain statistical information on the fluctuations of the laser modes, we perform a numerical integration of the stochastic differential equations given in the preceding section. From certain initial conditions, we follow the trajectory of the fields or intensities in time, introducing random fluctuations at each time step to account for the Langevin noise sources. Since in this paper we are interested in the fluctuations of the laser about the steady state, we first determine the steady-state average values of the intensities of the modes and the population inversion. This is accomplished in trial runs in which we calculate these average values that will serve as input for

TABLE I. Typical parameter values for $In_xGa_{1-x}As$:P.

Symbol	Parameter	Value
L	length	250 μm
V	volume	10^{-10} cm^3
A_{nr}	nonradiative recombination rate	10^8 s^{-1}
B	radiative recombination coefficient	10^{-10} cm^3/s
C_{Aug}	Auger recombination coefficient	5×10^{-29} cm^6/s
β_c	linewidth enhancement factor	6
A	gain coefficient	7500 s^{-1}
β_{sp}	spontaneous-emission factor	6×10^{-5}
β_{11} (β_{22})	mode self-saturation coefficients	5×10^4 s^{-1}
θ_{12},θ_{21}	mode cross-saturation coefficients	5×10^4 s^{-1}
F_{mm}	angular frequency mismatch between cavity mode and laser frequency	10^7
R_{sp}	spontaneous-emission rate	2×10^{12} s^{-1}
μ	group index refraction	4
γ_1,γ_2	loss	7.36×10^{11} s^{-1} (for internal loss of 50 cm^{-1} and mirror reflectivities of 0.3)

later simulations. In this section we describe the numerical integration procedure for the simulations and the techniques for calculating the correlation functions and various spectral quantities.

A fourth-order Runge-Kutta method was used for the numerical integration. This method allows us to take time steps as large as 10 psec. The central processing unit time taken for each trajectory (of lengths ranging from 50 000 to 250 000 steps) is kept reasonably low, at the same time maintaining a high level of accuracy in the solution of the deterministic part of the equations over a time step. On a CYBER 990, this implies a computation time of less than 100 sec for each trajectory. Ten to fifty trajectories are necessary to obtain reasonably precise statistical averages from the simulations.

The noise sources are simulated by the generation of Gaussian random numbers with noise strengths as stated in Sec. II. The Box-Mueller algorithm[14] was used to obtain Gaussian numbers from uniformly distributed random numbers. The technique of Marcuse was applied to establish a cross correlation between noise sources when necessary.[4] At each integration step the Gaussian random numbers with the correct variance are added to the deterministic part of the solution. This Monte Carlo procedure provides us with values of the field or intensity and phase for each time step. Statistical averages are then computed from these values.

The correlation functions are determined by taking the product of variables with the appropriate time delay over the entire range of the trajectory and then averaging. To ensure sufficient accuracy in the values of the correlation functions, the individual trajectories must be many times longer than the maximum delay for which the correlation functions are computed.

A fast Fourier transform (FFT) was used to calculate spectra. The Nyquist frequency

$$f_c = 1/2\Delta \tag{24}$$

where Δ is the integration time step determines the highest frequency of the spectrum. The frequency resolution available from the simulations is given by

$$\Delta f = 1/N_s\Delta \tag{25}$$

where N_s is the total number of time steps in the trajectory.

IV. INTENSITY FLUCTUATIONS

In this section we will present the results of our simulations on the intensity fluctuations of the two-mode laser. There are many different measures of intensity noise that convey information on somewhat different aspects of laser behavior. The auto- and cross-correlation functions of the two modes will be calculated first; they specify the time scales of the coherence properties of the laser. They also demonstrate how the fluctuations of the main and side mode are related. The values of the autocorrelation functions of the modes at zero time delay (the normalized variance of the intensity) are a measure of the "total noise" of the laser. The change of this variance with injection current from operation below threshold to above threshold describes graphically the disorder-order "phase transition" in the properties of the laser light. The power spectrum of the intensity fluctuations relative to the mean steady-state intensity, often called the relative intensity noise (RIN), provides information on the frequency content of the fluctuations. We will also compare the results of the linearized theory with the simulations whenever possible.

In Fig. 1(a) we show part of an intensity time trace for the main and side modes. A large mode-suppression ratio ($M \equiv P_2/P_1$) of 0.13 has deliberately been chosen to illustrate the effect of mode partitioning. The value of the parameter β_{sp} (determined by the guiding mechanism of the laser which varies normally between 10^{-4} and 10^{-5} for index guided lasers[2]) was 2×10^{-4}; it is this pa-

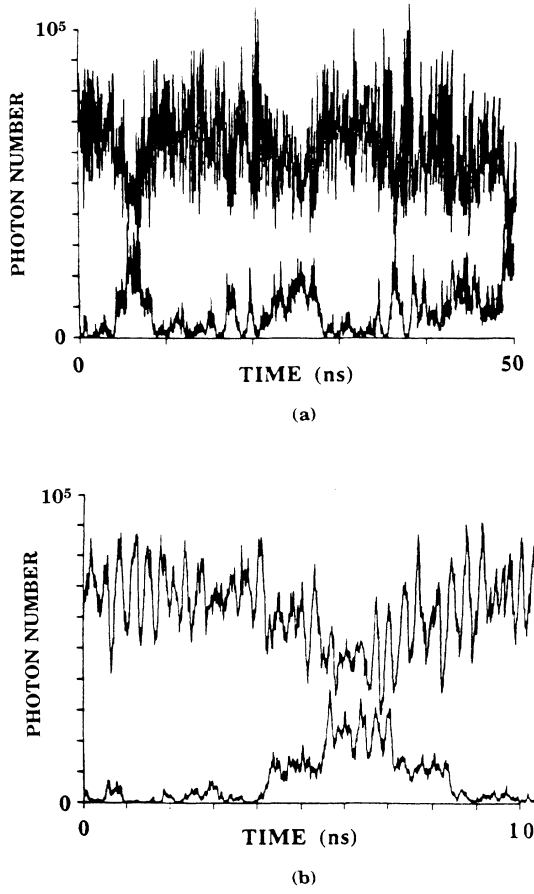

FIG. 1. (a) Time trace of the intensity of the semiconductor-laser main and side modes at an injection current $I=24$ mA and a mode-suppression ratio of 0.13. Mode-partition effects and anticorrelation between the two modes are clearly seen. (b) An expanded view of the first 10 ns of (a) that shows the laser relaxation oscillations.

rameter that determines the mode-suppression ratio if the losses are taken to be equal for both the modes. The mode-suppression ratio is also affected by the width of the gain curve relative to the mode spacing; the latter is determined by the length of the laser and the group index of refraction of the medium. In our simulations we have used three different gain curve widths corresponding to the situations where 21, 35, or 61 cavity resonances lie underneath the gain curve. An alternate mechanism for changing the mode-suppression ratio is to have a frequency-dependent loss. This is the technique adopted in distributed feedback lasers. The intensity fluctuations due to the noise sources are rather prominent for the operating point selected, i.e., fairly close to threshold. The mode-partition effect consists of the sharing of power between the modes; they fluctuate in such a way as to keep the total power approximately constant. Thus, when the intensity of mode 1 decreases, the intensity of mode 2 is seen to increase and vice versa. Figure 1(b) shows an expanded view of the first 10 nsec of Fig. 1(a). Note the ringing of the main mode, due to relaxation oscillations in which energy is exchanged between photons and carriers. Oscillations are also seen in the side mode when its amplitude is appreciable.

The intensity correlation functions for the two modes are defined as

$$C_{ij}(\tau)=\int_{-\infty}^{+\infty}\frac{\delta P_i(t+\tau)\delta P_j(t)}{\langle P_i\rangle\langle P_j\rangle}dt$$
$$=\frac{\langle\delta P_i(t+\tau)\delta P_j(t)\rangle}{\langle P_i\rangle\langle P_j\rangle}\,, \tag{26}$$

where i and j take the values of the mode indices; C_{11} and C_{22} are autocorrelations, while C_{12} is the cross-correlation function. δP_i are the deviations from the mean intensities and τ is the time delay. The autocorrelation function for the total power $C_T(\tau)$ is defined similarly. The total power output of the laser is obtained by first adding the complex amplitudes of the main and side mode fields (taking into account the difference in frequency of the two modes) and then finding the absolute value squared of the total electric field. This leads to beating between the two modes, which is evident in correlation functions and power spectra for the total power of the laser. In Figs. 2(a)–2(c) are shown the autocorrelation functions $C_{11}(\tau)$ and $C_T(\tau)$ for the main mode and the total intensity, as well as the cross-correlation function $C_{12}(\tau)$ for the main and side mode. We note that $C_T(\tau)$ shows rapid oscillations due to intermode beating at a frequency of about 150 GHz for an assumed laser length of 250 μm and group refractive index of 4. The cross correlation is negative in Figs. 2(b) and (c), indicating anticorrelated fluctuations of the two-mode intensities. In Figs. 2(b) and 2(c) we show only $C_{11}(\tau)$ and $C_{12}(\tau)$. In Fig. 2(a), for the smallest M (0.001), the cross-correlation function oscillates, taking both positive and negative values. As the mode-suppression ratio is decreased, it becomes increasingly important to average over a large number of trajectories to obtain the cross-correlation function with a given precision. All three functions ring at the relaxation oscillation frequency and approach zero at long time delays. The correlations die out within a couple of nanoseconds. Though not shown in Figs. 2(b) and 2(c), the total power correlation function dies out more slowly as the side mode strength is increased. The correlation functions for the side mode are shown in Figs. 2(d) and 2(e) for M values of 0.01 and 0.2, respectively. They are completely different in character from the main mode autocorrelations, showing very little trace of the relaxation oscillations. The decay is approximately exponential and its time scale is similar to that for the envelope of Fig. 2(a).

To increase the mode-suppression ratio, we have used a larger value of β_{sp} than before and have increased the width of the gain curve [there are 21, 35, and 61 modes under the gain curve for Figs. 2(a)–2(c), respectively]. We notice from Figs. 2(a)–2(c) that the values of the auto- and cross-correlations grow appreciably larger in magnitude for zero time delay, indicating a larger level of

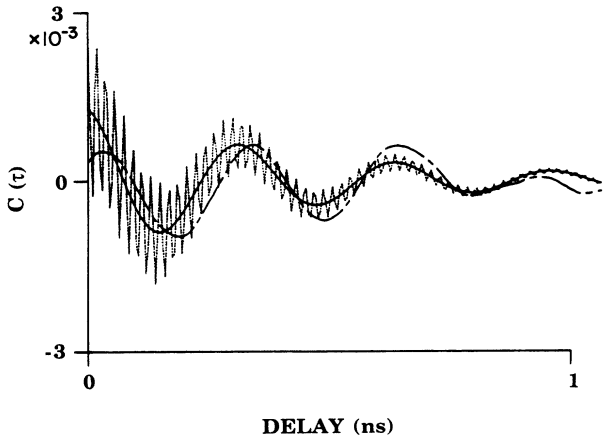

(a)

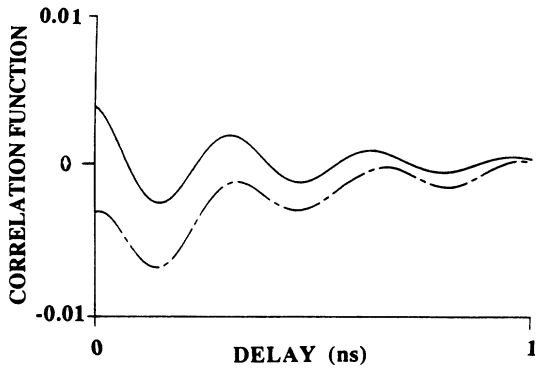

(b)

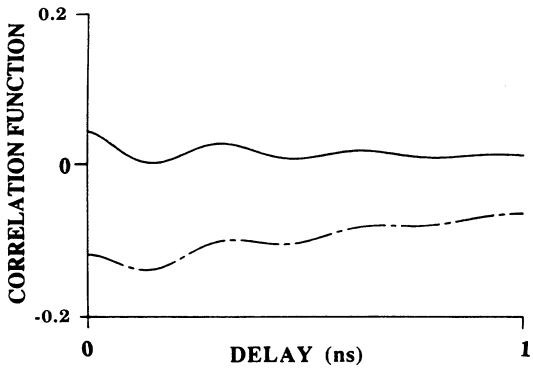

(c)

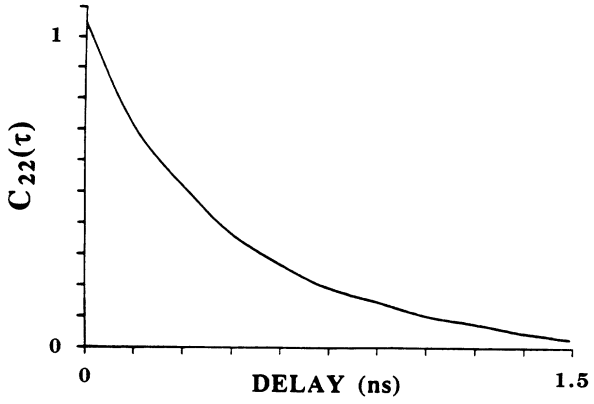

(d)

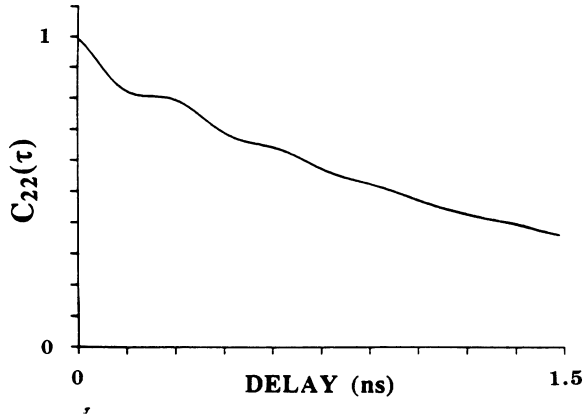

(e)

FIG. 2. (a) Intensity autocorrelation functions for the total intensity (· · · ·), main mode intensity (——), and the cross-correlation function (— - — -) between the main and side modes. The injection current is $I = 24$ mA. The mode-suppression ratio M is ≈ 0.001. (b) $M \approx 0.01$ and only the main mode autocorrelation and cross-correlation between main and side modes are shown. (c) $M \approx 0.2$ and only the main mode autocorrelation and cross-correlation between main and side modes are shown. (d) Side mode autocorrelation function for $M \approx 0.01$. (e) Side mode autocorrelation function for $M \approx 0.2$.

intensity fluctuations. The increased magnitude of the anticorrelation of the main and side mode demonstrates the mode-partitioning effect; in fact the "mode-partition coefficient" k is defined commonly by[12]

$$k^2 = -C_{12}(0) . \tag{27}$$

At zero time delay, the autocorrelation functions reduce to the normalized variance of the photon number. The change in this variance with injection current (for the main mode and total power) as the laser is taken from below threshold operation to far above threshold represents the approach to the coherent state. Below threshold, $C_{11}(0)$ is approximately unity. Far above threshold, it asymptotically approaches zero. As seen in Fig. 3(a), with $M=0.002$, the transition to threshold is very sharply defined. The limiting value below threshold of $C_T(0)$ is also unity. Above threshold it very closely follows the behavior of the main mode variance. The side mode variance, on the other hand, stays at approximately unity over the entire range of operation of the laser. It is well known that the normalized variance for light from a thermal source is unity.[15]

If the mode-suppression ratio is increased to 0.1, the transition across the laser threshold is noticeably broader. Instead of a sharp decline in $C_{11}(0)$ and $C_T(0)$ as the injection current is increased, we now have a gradual decrease in the normalized variances. Laser threshold can no longer be precisely defined. Further, the laser needs to be driven at higher injection currents to reduce the variance to values below 0.01, even though the total power output is the same as before for a given injection current. In contrast to Fig. 3(a), the value of $C_T(0)$ is significantly higher than the corresponding value of $C_{11}(0)$. This is particularly noticeable at higher injection currents.

It is important to note that a linearized treatment of the two-mode laser cannot predict the behavior near the threshold region. Our computer simulations provide a technique to quantitatively probe the fluctuations in this regime, where a transition from a disordered state to an ordered state occurs. The effect of the side mode on the transition across the threshold is significant even when the side mode is 20 times smaller in power than in the main mode.

Figure 3(c) demonstrates the inadequacy of the linearized theory to predict the fluctuations near threshold of a purely single-mode laser. Above threshold, the agreement of the simulation results with the linearized theory is excellent. Near threshold, the deviation is evident. The variance is obtained from the linearized theory by integration of the normalized power spectrum over the entire frequency range.[16] Also shown for comparison is the variance of the total power of a two-mode laser ($M \sim 0.1$); this variance is considerably larger than for a single-mode laser.

The relative intensity noise is an important quantity that specifies the frequency components in the intensity fluctuations. It is defined in terms of the Fourier transform of the autocorrelation functions of Eq. (26):

$$R(\omega) = \int_{-\infty}^{\infty} \frac{\langle \delta P_i(t+\tau)\delta P_i(t)\rangle e^{-i\omega\tau}}{\langle P_i\rangle^2} d\tau . \tag{28}$$

The use of the Wiener-Khinchin theorem allows us to express the RIN for a stationary stochastic process as[17]

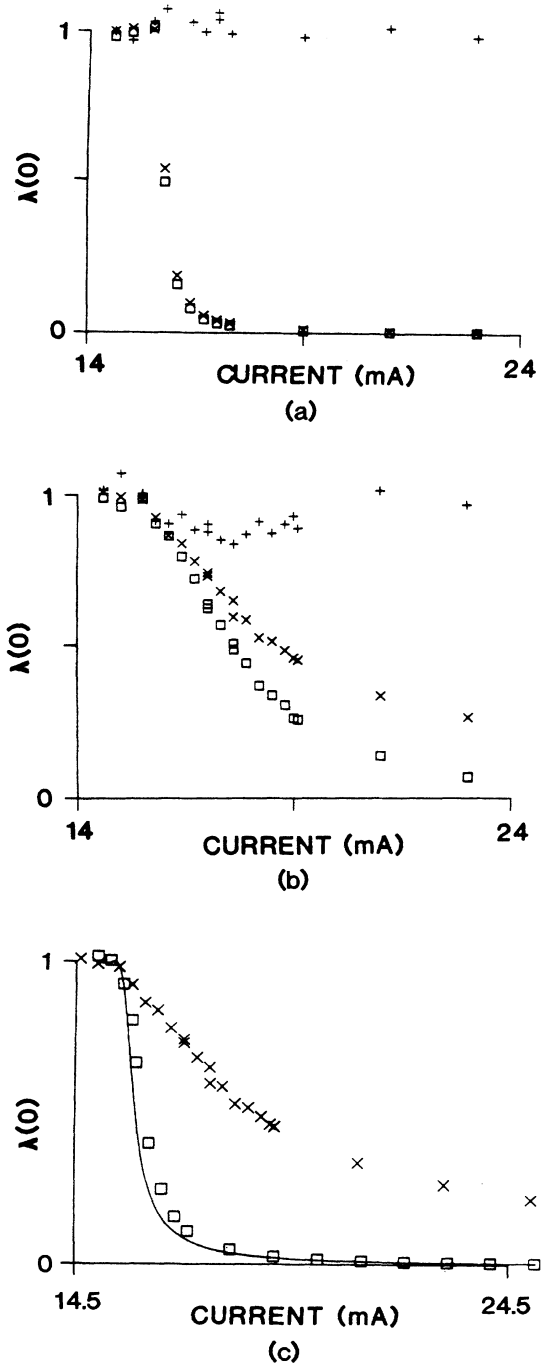

FIG. 3. Normalized variance of the main mode (□), side mode (+), and total intensity (×) vs injection current I. (a) $M \approx 0.002$, (b) $M \approx 0.1$, (c) a comparison of the linearized theory for a single-mode laser with numerical results for a purely single-mode laser and for a two-mode laser ($M \approx 0.1$). Theory (——), single-mode simulation (□), two-mode simulation (×).

$$R(\omega)=\frac{\left|\int_{-\infty}^{\infty}\delta P_i(t)e^{-i\omega t}dt\right|^2}{\langle P_i\rangle^2}=\frac{\langle|\delta P_i(\omega)|^2\rangle}{\langle P_i\rangle^2}\ , \tag{29}$$

where $\delta P_i(\omega)$ is the Fourier transform of $\delta P_i(t)$. The calculation of the RIN from the computer simulations can then be carried out as follows. In the limit that the total integration time $T\rightarrow\infty$ the RIN is given by

$$R(\omega)=\frac{1}{T}\frac{\left|\sum_n\delta P_i(t_n)e^{-i\omega_n t_n}\Delta\right|^2}{\langle P_i\rangle^2}$$

$$=\frac{\Delta^2}{T\langle P_i\rangle^2}|\mathcal{F}(\delta P_i(t))|^2\ , \tag{30}$$

where we have replaced the integral by a discrete sum. $\mathcal{F}$ stands for the fast Fourier transform and Δ is the time step for the integration. Thus we take the FFT of a time trajectory of the photon number and use Eq. (30) to obtain the RIN. The uncertainty associated with the RIN so calculated can be reduced by averaging over large numbers of trajectories.

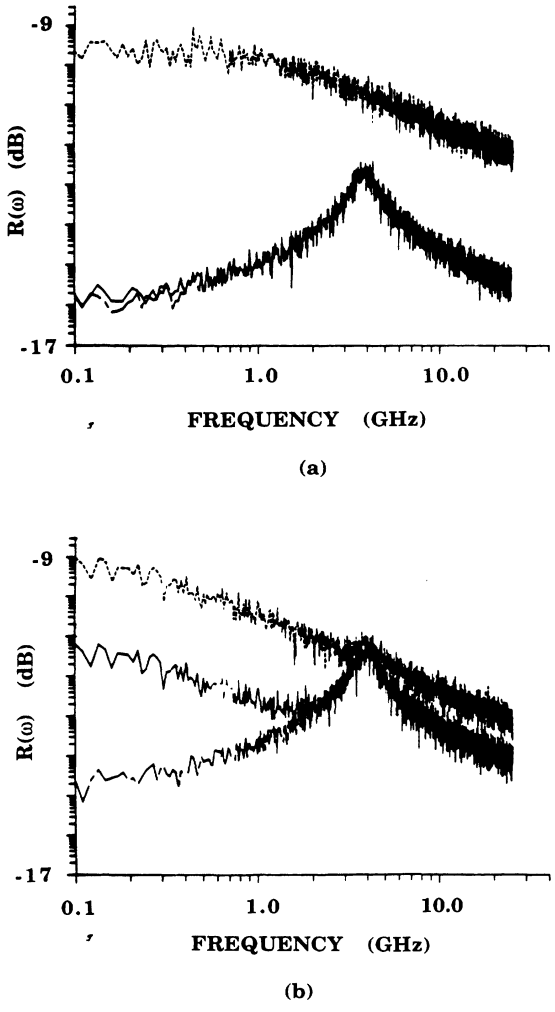

FIG. 4. Relative intensity noise spectra (RIN) for $I=28$ mA for the main mode (——), side mode (· · · ·), and total intensity (— - — -). (a) $M\approx0.0008$. (b) $M\approx0.06$.

Figures 4(a) and 4(b) show the main mode, side mode, and total power RIN's for operation well above threshold and for two different values of M. When M is small [0.008 in Fig. 4(a)] the main mode and total power RIN's are essentially identical in the range of frequencies considered. We can see clear evidence of the relaxation oscillations in the peaks of the spectra, located at about 4 GHz for an injection current of 28 mA. The side mode RIN, on the other hand, shows no such peak, but decays from an initial value about six orders of magnitude higher. In Fig. 4(b) $M=0.06$. Now the main mode and total power RIN's are well separated initially in the frequency range below 1 GHz. This is caused by mode-partition noise, in which the main and side modes fluctuate in an anticorrelated fashion, resulting in much smaller fluctuations in the total mode power. Both main mode and total power RIN's still peak at the relaxation oscillation frequency, and now a small peak is also observed in the RIN of the side mode at this frequency, corresponding to the relaxation oscillations seen in the side mode intensity in Fig. 1(b). In these figures we have restricted ourselves to a frequency range below the beat frequency of the two modes. If we looked at high enough frequencies, there would be a peak in the RIN for the total power at the beat frequency.

When the laser is operated closer to threshold, the relaxation oscillation peak shifts to lower frequencies, as predicted theoretically.[2] Thus the behavior of the RIN seen in our simulations is generally as expected from previous experiments and theory.

V. FIELD FLUCTUATIONS

Computer simulation of the stochastic equations (1), (2), and (8) allow us to obtain information on the field fluctuations as well as intensity noise. Whereas there have been previous studies of intensity noise[4–10] that complement our results reported here, there have been no direct computations of the field fluctuations to our knowledge.

The lineshape or field spectrum of the laser is the Fourier transform of the complex field autocorrelation function defined mathematically as

$$L_i(\omega)=\int_{-\infty}^{\infty}\langle E_i^*(t+\tau)E_i(t)\rangle e^{-i\omega\tau}d\tau\ , \tag{31}$$

where the subscript i denotes the main or side mode. The line shape of the laser can be experimentally determined with the Fabry-Perot interferometer or by an optical heterodyne method which results in a beat spectrum between the test laser and a reference laser field. The field spectrum may be calculated in a linearized approach;[18] a restriction of this procedure is that the contribution of intensity fluctuations to the line shape must be neglected. Also, the method is prohibitively complicated if more than one mode is considered.

An advantage of our technique is the ability to calculate the line shape including the effect of the intensity

fluctuations. The technique also works equally well for a multimode laser as it does for a single-mode laser. The simplicity of our technique for computation of the line shapes is due to the use of the electric field equations for the integration. The absolute value squared of the FFT of the electric field [analogous to Eq. (29)] directly results in the line shape.

Figure 5 shows the main and side mode line shapes for $M=8\times10^{-4}$. The main mode spectrum is Lorentzian in the center, as is shown by the least-squares-fit curve (dashed line). The two prominent satellite peaks are due to the relaxation oscillations. Their frequency shift relative to the central peak is proportional to the square root of the power in the main mode.[1] A faint trace of two higher-order satellite peaks is seen in the wings of the main mode line shape. The side mode spectrum is Lorentzian, and shifted from the cavity resonance by about 3 GHz. A simple calculation for a laser below threshold that neglects fluctuations in the population inversion gives the following result for the line shape:[1]

$$L_i(\omega)=\frac{R_{sp}}{[\omega_0+(\beta_c/2)(G-\gamma)-\omega]^2+(G-\gamma)^2/2} . \quad (32)$$

From this equation the frequency shift is seen to be

$$\delta_\nu=\frac{\beta_c}{4\pi}(G-\gamma)\simeq\beta_c\frac{R_{sp}}{4\pi P} , \quad (33)$$

where in the last step we have replaced $G-\gamma$ by its steady-state value R_{sp}/P from Eq. (16). It accurately predicts the shift of the side mode or of the main mode as a function of its power. The shift (measured from the high power limit central frequency) is large below threshold and decreases to zero as the photon number in the mode grows.

Figure 6 is an expanded view of the satellite peaks that shows clearly the asymmetry in their size. As has been discussed by Vahala, Harder, and Yariv,[19] this asymmetry is the result of the coupling between the amplitude and phase fluctuations. Our computations reveal this effect naturally since we automatically incorporate this coupling in our equations. This asymmetry is found over the wide range of M values that we have investigated.

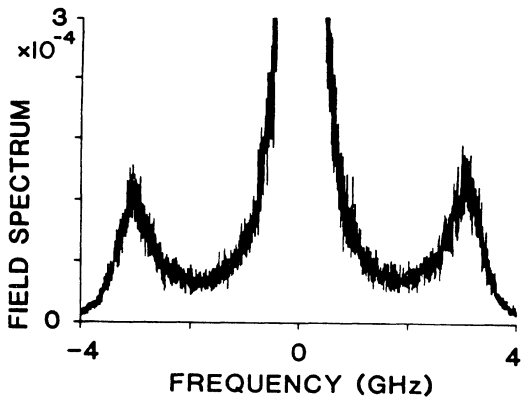

FIG. 6. Relaxation oscillations for the main mode line shape for $I=24$ mA and $M\approx0.001$. Note the asymmetry of the sidebands which arises from the coupling of the phase and intensity fluctuations.

In Fig. 7, we have shown the main mode spectrum of a laser slightly above threshold. Multiple relaxation oscillation peaks are seen in this regime of operation, which cannot be treated accurately with a linearized theory.

Looking back at Fig. 5, we note that the wings of the main mode spectrum fall far below the Lorentzian profile that fits the central portion of the line shape. This falloff of the line shape is caused by the damping of the relaxation oscillations[18] (which depend on the gain saturation terms and the decay rate of the population inversion). If we neglect the nonlinear gain or saturation terms [i.e., we set the β and θ factors to zero in Eqs. (5) and (6)] then the relaxation oscillations are much less damped and the line shape fits the Lorentzian slightly better in the wings. This is shown in Fig. 8.

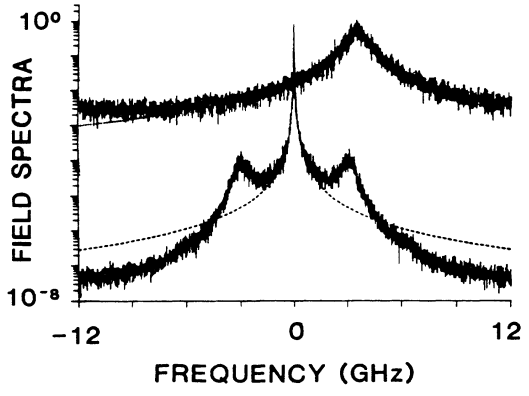

FIG. 5. Line shapes for the main mode (centered at 0) and side mode for $I=24$ mA and $M=0.0008$. Also shown are Lorentzian fits for the main mode (— — —) and for the side mode (· · · ·).

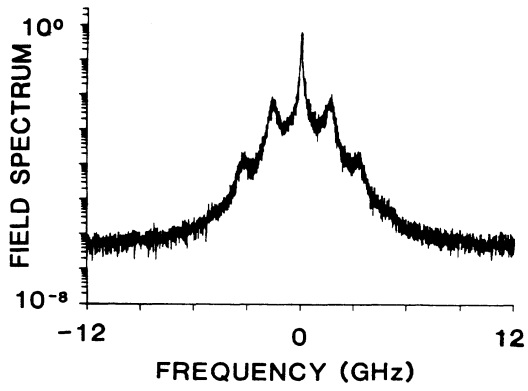

FIG. 7. Main mode line shape for $I=18$ Ma ($I_{th}=16$ mA) for $M\approx0.001$.

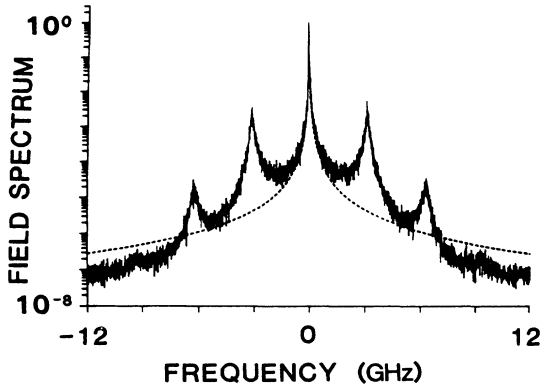

FIG. 8. Main mode line shape with self- and cross-saturation coefficients set to zero. Note the underdamped relaxation oscillations and the Lorentzian fit to the central peak (— — —).

The laser main mode linewidth can be determined by a Lorentzian least-squares fit to the line shape obtained from the simulations. Only the portion of the line shape within a GHz of the line center was included for these fits. Thus the effect of the relaxation oscillation satellite peaks was negligible in the determination of the linewidth, which is defined as the full width at half maximum of the Lorentzian fit. A weighting procedure that attributes a higher weight to the wings was used; this gave us less uncertainty in the final linewidth.

In Figs. 9(a)–9(c) we show the variation of the linewidth as a function of the inverse power of the main mode. The Schawlow-Townes formula for the semiconductor-laser linewidth, as modified by Henry,[1] is

$$\Delta\nu=\frac{R_{\rm sp}}{4\pi P_1}(1+\beta_c^2)\ , \tag{34}$$

where all the quantities involved have been previously defined. A linear plot is expected from this equation, and is shown as a dashed line for the parameter values used in the simulations. The solid line is a linear least-squares fit to the data points (squares) obtained from the simulations. The mode-suppression ratio increases from 0.001 [Fig. 9(a)] to 0.01 [Fig. 9(b)] and finally, to 0.15 [Fig. 9(c)]. The plots remain very linear through this progression, but deviate more from the straight lines obtained from Eq. (34). Furthermore, the intercept on the vertical axis as obtained from the linear regression becomes noticeably nonzero for the mode-suppression ratio of 0.15. In Fig. 9(c), this intercept is 7.7±5.4 MHz. This would seem to indicate that a contribution to the power-independent linewidth may arise from the existence of a second mode. This conclusion has also been reached earlier by Elsasser and Goebel[20] and by Miller[21] by different techniques.

VI. DISCUSSION

The study presented here defines the limits of applicability of the linearized single-mode semiconductor-laser theory. Our results show that the linearized theory is accurate to within a few percent far below threshold (output power in the microwatt regime), as well as above threshold (output power greater than a milliwatt). Con-

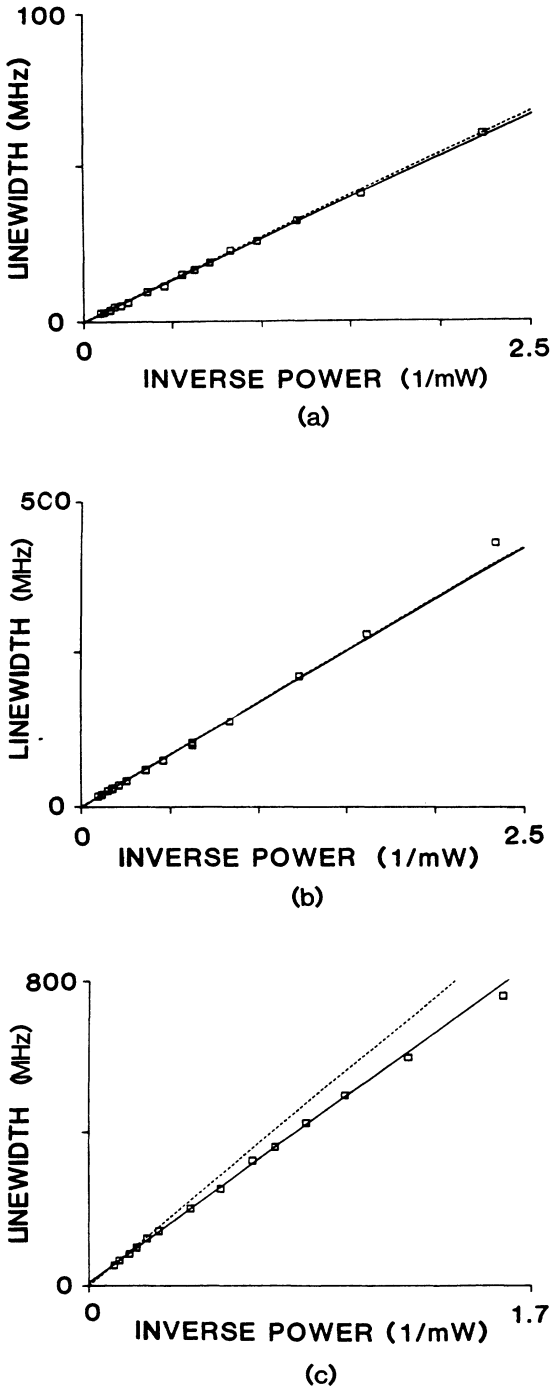

FIG. 9. Linewidth of the main mode vs inverse power for three different mode-suppression ratios. The computed values are shown by the squares. The solid line is a linear least-squares fit to the computed values, while the dashed line is from Eq. (34). (a) $M\approx 0.001$. (b) $M\approx 0.01$. (c) $M\approx 0.15$.

siderable discrepancies of the numerical calculations with the analytic theory are found in the intermediate regime. The agreement of the Monte Carlo results above threshold with both experimental results and linearized theory emphasizes the correctness and accuracy of the technique and lends credence to the results obtained in the threshold regime.

Though the single-mode theory of the semiconductor laser is adequate for many purposes, it is important to realize that a "single-mode" laser often has a second mode of smaller intensity which contributes appreciably to the fluctuations of the main mode. It is much more difficult to account for this situation with an analytic theory. Our numerical technique allows us to consider arbitrary mode-suppression ratios and compute the effects of mode partition on both the intensity and field fluctuations. We have demonstrated here the ability of the Monte Carlo procedure to provide accurate results on the laser line shape, accounting for the coupling between the intensity and phase fluctuations in a two-mode laser.

In the future, we will apply this method of calculation to problems that involve noise and the nonlinear dynamics of semiconductor lasers, including the important practical question of external reflections into the laser cavity.

ACKNOWLEDGMENTS

We thank Govind Agrawal for stimulating discussions and assistance at all stages of this research. R. R. would like to thank C. H. Henry and R. F. Kazarinov for sharing their insights on semiconductor lasers and their hospitality at AT&T Bell Laboratories. This work was supported by National Science Foundation Grant No. ECS-8722216.

[1]C. H. Henry, IEEE J. Lightwave, Tech. **LT-4**, 298 (1986).
[2]G. P. Agrawal and N. K. Dutta, *Long Wavelength Semiconductor Lasers* (Van Nostrand Reinhold, New York, 1986).
[3]C. H. Henry and R. F. Kazarinov, IEEE J. Quantum Electron. **QE-22**, 294 (1986).
[4]D. Marcuse, IEEE J. Quantum Electron. **QE-20**, 1139 (1984).
[5]D. Marcuse, IEEE J. Quantum Electron. **QE-20**, 1148 (1984).
[6]D. Marcuse, IEEE J. Quantum Electron. **QE-21**, 161 (1985).
[7]S. E. Miller, IEEE J. Quantum Electron. **QE-21**, 1644 (1985).
[8]S. E. Miller, IEEE J. Quantum Electron. **QE-23**, 1071 (1987).
[9]S. E. Miller, IEEE J. Quantum Electron. **QE-24**, 750 (1988).
[10]N. H. Jensen, H. Olesen, and K. E. Stubkjaer, IEEE J. Quantum Electron. **QE-23**, 71 (1987).
[11]M. Osinski and J. Buus, IEEE J. Quantum Electron. **QE-23**, 9 (1987).
[12]G. P. Agrawal, Phys. Rev. A **37**, 2488 (1988).
[13]M. Lax, in *Brandeis Lectures,* edited by M. Chretien, E. P. Gross, and S. Deser (Gordon and Breach, New York, 1968), Vol. II.
[14]D. E. Knuth, *Seminumerical Algorithms,* Vol. 2 of *The Art of Computer Programming* (Addison-Wesley, Reading, MA, 1981).
[15]J. W. Goodman, *Statistical Optics,* (Wiley, New York, 1985).
[16]C. H. Henry, P. S. Henry, and M. Lax, IEEE J. Lightwave Tech. **LT-2**, 209 (1984).
[17]W. H. Press, B. P. Flannery, S. A. Teukolsky, and W. T. Vetterling, *Numerical Recipes* (Cambridge University Press, Cambridge, England, 1986).
[18]C. H. Henry, IEEE J. Quantum Electron. **QE-19**, 1391 (1983).
[19]K. Vahala, C. Harder, and A. Yariv, Appl. Phys. **42**, 211 (1983).
[20]W. Elsasser and E. O. Goebel, IEEE J. Quantum Electron. **QE-21**, 687 (1985).
[21]S. E. Miller, IEEE J. Quantum Electron. **24**, 1873 (1988).